Role of Sr on microstructure, mechanical properties, wear and corrosion behaviour of an Al–Mg$_2$Si–Cu in-situ composite

Saeed Farahany [a,*], Hamidreza Ghandvar [b], Mansour Bozorg [c], Azmah Nordin [d], Ali Ourdjini [e], Esah Hamzah [b]

[a] Department of Chemical and Materials Engineering, Buein Zahra Technical University, 3451745346, Qazvin, Iran
[b] Department of Materials, Manufacturing and Industrial Engineering, Faculty of Mechanical Engineering, Universiti Teknologi Malaysia (UTM), 81310, Johor Bahru, Malaysia
[c] Faculty of Chemical and Materials Engineering, Shahrood University of Technology, Iran
[d] Malaysia-Japan International Institute of Technology (MJIIT), Universiti Teknologi Malaysia, 54100, Kuala Lumpur, Malaysia
[e] Department of Mechanical Engineering, Faculty of Engineering, University of Ottawa, Ontario, Canada

HIGHLIGHTS

- Effect of strontium addition on primary and eutectic Mg$_2$Si was evaluated.
- The most desirable modification was achieved with addition of 0.01 wt% Sr.
- Modification and de-modification mechanisms with increase of Sr were proposed.
- Tensile, impact, fracture, wear and corrosion properties were studied.

ABSTRACT

The influence of Sr additions on the microstructure of primary and eutectic Mg$_2$Si phases, wear and corrosion behaviour of Al–Mg$_2$Si–Cu in-situ composite was investigated. The results showed that addition of 0.01 wt% Sr modified the primary Mg$_2$Si morphology but exceeding this level of Sr induced a loss of modification as the primary phase morphology coarsened again. The Al–Mg$_2$Si eutectic phase, on the other hand, still exhibited a refined structure even with higher levels of Sr additions. Thermal analysis results revealed that both modification of the primary Mg$_2$Si and refinement of the eutectic Mg$_2$Si are most likely related to nucleation and growth stages respectively. The results of 0.01 wt% Sr addition showed that the mean size and mean aspect ratio decreased by about 30% and 6% respectively, but the mean density increased by 185% respectively. The highest UTS, El%, impact toughness and hardness were measured at 101.57 MPa, 1.1%, 1.31 J and 81 VHN respectively. Fractography of tensile and impact specimens from the Sr-treated composite revealed that Mg$_2$Si particles suffered cracking with few decohesion indicating higher ductility. The results of wear testing also showed that composites treated with Sr have higher wear resistance compared with those of without Sr. The highest resistance to wear was observed in the composite containing 0.01 wt %Sr which is likely the result of good dispersion of fine Mg$_2$Si particles in the Al matrix. This fine morphology and uniform distribution of Mg$_2$Si particles also contributed to better corrosion resistance by reducing the propagation of corrosion pits.

1. Introduction

The term "in-situ metal matrix composite" refers to a specific class of composite materials consisting of a continuous metallic matrix reinforced with a second phase that is formed in situ during solidification. The motivation behind the fabrication and use of in-situ metal matrix composites (MMCs) lies in the fewer production steps and reduction of production cost. Moreover, wetting of the reinforcement by the matrix is improved [1] and matrix/reinforcement interfaces are stable. Al–Mg$_2$Si MMCs have the potential to replace the commonly used hyper-eutectic Al–Si alloys. The characteristics of Mg$_2$Si reinforcement particles play a major role in carrying a high portion of the stress when the composite

is subjected to an external load, and hence to achieve superior mechanical properties. However, the coarse and dendritic morphology of Mg_2Si particles with sharp edges in the as-cast condition are detrimental to the mechanical properties of Al–Mg_2Si in-situ MMCs. Hence, several researches have been carried out to alter the morphology of these primary Mg_2Si particles. Zhao et al. [1] was the first to have reported that Al–Sr master alloy can modify the primary Mg_2Si in in-situ Mg_2Si/Al–Si–Cu composite. Qin et al. [2] reported similar results with the addition of 0.05, 0.1 and 0.15 wt% Sr and also discussed the formation of the cubic primary Mg_2Si particles. In their work of the effects of Sb and Sr additions on AZ61-0.7Si alloy, Ming-bo et al. [3] observed that 0.12% Sr altered the primary Mg_2Si phase from coarse Chinese script morphology to fine granule and/or irregular polygonal shape. Most research available in the literature has so far focused on morphological evolution and growth mechanism of primary Mg_2Si.

Dongtao et al. [4] investigated the influence of Sr on microstructural features of Al–25Mg_2Si and reported that the highest hardness and tensile values were obtained with 0.05 wt% Sr addition. On the other hand, Wu et al. [5] also been noted that the wear rates and friction coefficient of the Nd-modified Al–18Mg_2Si composites are lower than the Nd-free composite, whereas, Zedi Li et al. [6] showed that addition of Al–P master alloy enhances the corrosion resistance of Al–20Mg_2Si. Moreover, it has been reported that subjecting the composite to heat treatment resulted in suppressing the rapid expansion of corrosion pits and hence enhancing the corrosion resistance of Al–10Mg_2Si alloy [7]. It is evident that the characteristics of Mg_2Si particles have a significant effect on the properties of in-situ Al–Mg_2Si MMCs, i.e. mechanical, wear and corrosion characteristics. However, there is limited systematic research available in the literature. The aim for this paper is to examine the relationship between the microstructure and properties of the produced Al–20Mg_2Si–2Cu in-situ composite after addition of strontium. Moreover, computer-aided cooling curve thermal analysis (CA-CCTA) was performed to identify the mechanism responsible for the modification of primary and eutectic Mg_2Si particles.

2. Experimental procedure

The Al–20Mg_2Si–2Cu test alloys were prepared by melting commercially ADC12 alloy and high purity (>99.99 wt %) of aluminium and magnesium in a silicon carbide crucible in an induction furnace. The chemical composition of the composite investigated is listed in Table 1.

After melting and degassing, strontium was added in the form of an Al–10Sr master alloy. The nominal strontium contents of the five test alloys were 0, 0.01, 0.04, 0.08 and 0.1 wt %. After holding for 5 min to allow for homogenisation the melt was skimmed and poured into pre-heated mild steel permanent moulds to fabricate tensile and impact test specimens. Parallel to casting test samples, around 200 gr of melt was poured in pre-heated ceramic mould for thermal analysis. The temperature-time data was recorded using an EPAD-TH8-K high-speed data acquisition system linked to a computer with DEWESoft 7.5 at a dynamic rate of 100 Hz/ch. FlexPro10 data analysis software was used for smoothing the curves and plotting the cooling curve, first (dT/dt) and second derivative (d^2T/dt^2) curves for the extraction of thermal information. The cylindrical tensile test bars were produced out of the solidified rods and prepared according to ASTM B557M-10. Tensile testing was performed on an Instron testing machine (5982) at a constant crosshead speed of 1.0 mm/min. The V-notch impact specimens were cut using EDM wire cut machine in order to obtain the desired rectangular shape according to ASTM E23-12c. The impact test was

carried out using the Zwick impact tester with a 15-J hammer. Vickers hardness (Matsuzawa DVK-2) was measured using a load of 5 N. Dry sliding wear tests were conducted according to ASTM: G99 - 05 standard in a pin-on-disc wear testing apparatus (Ducom, TR20-LE). The pins with 6 mm in diameter and 25 mm in length were prepared by machining the samples, which were ultrasonically cleaned prior to testing. The following test parameters were used for all samples: 5 N and 20 N for the normal load, 0.628 m/s for the sliding speed, 2000 m for sliding distance and 30 mm for track radius of the rotating steel disc as counter face which was hardened to 60HRC. Wear resistance was evaluated by measuring the friction coefficient, wear rate and weight loss. The friction coefficient was attained by dividing the friction force to applied load. The average weight loss of the samples was measured by a microbalance with accuracy of 0.01 mg. The values reported are the average of three test samples for every experimental condition.

Rectangular specimens with a surface area of 1 cm^2 were molded into epoxy resin for electrochemical tests. The test was conducted at 25 °C in open air, within a glass cell containing 350 ml of 3.5% NaCl solution using a PARSTAT 2263 potentiostat/galvanostat (Princeton Applied Research). A three-electrode cell was used for polarisation tests: the reference electrode being saturated calomel electrode (SCE), the counter electrode being a graphite rod, and the working electrode being the specimen. All experiments were carried out at a constant scan rate of 0.2 mV/s, from −250 mV to +250 mV related to the open circuit potential. The immersion tests of the specimens were conducted according to the G31-72 standard. Thirty rectangular specimens with a size of 15 mm × 20 mm × 5 mm were cut and subsequently ground with 400–2000 grit SiC papers. The specimens were then washed entirely with distilled water, rinsed, ultrasonically degreased with ethanol, and then dried at room temperature. The specimens were then immersed into a beaker containing 3.5% NaCl solution. The beakers were sealed with a pH value of 0.6, and incubated at a constant temperature of 25 °C for 25 days duration. Afterwards, the specimens were rinsed with acetone, deionized water, and corrosion products were removed before weight measurement. The corrosion rate was calculated as follows:

$$CR = \frac{534 \ W}{Adt} \tag{1}$$

where CR is the corrosion rate (mpy), W is mass loss (mg), A is surface area exposed to the corrosive media (in^2), t is exposure time (h), and d is density (g/cm^3).

Samples for microstructural characterisation of the cast samples were prepared using standard metallography procedures. First, the samples were ground using silicon carbide papers with different grit sizes and then were subjected to a final polishing with colloidal silica suspension (5 μm). Examination of the microstructures was performed using a Nikon-MIDROPHOT-FXL microscope after chemical etching with 2% HF acid for 5 s. The specimens were also subjected to deep etching for 6 h in a solution of 5% HCl acid and 95% ethanol in order to remove the aluminium matrix and examine the 3-D morphology of the Mg_2Si phase. The microstructures, fracture surfaces, worn surfaces, and the corroded surfaces were examined by field emission scanning electron microscopy (FESEM, Supra-35VP, Carl Zeiss, Germany), coupled with energy dispersive spectroscopy (EDS) facilities. The size, density, and aspect ratio of the primary Mg_2Si particles were quantitatively evaluated using an i-Solution image analyser.

3. Results and discussion

3.1. Microstructure

Fig. 1 illustrates the optical microstructures of as-cast Al–20Mg_2Si–2Cu composites with different amounts of Sr. There is evidence that morphological changes in both primary and eutectic Mg_2Si particles after addition of Sr were obtained. It can be seen that the
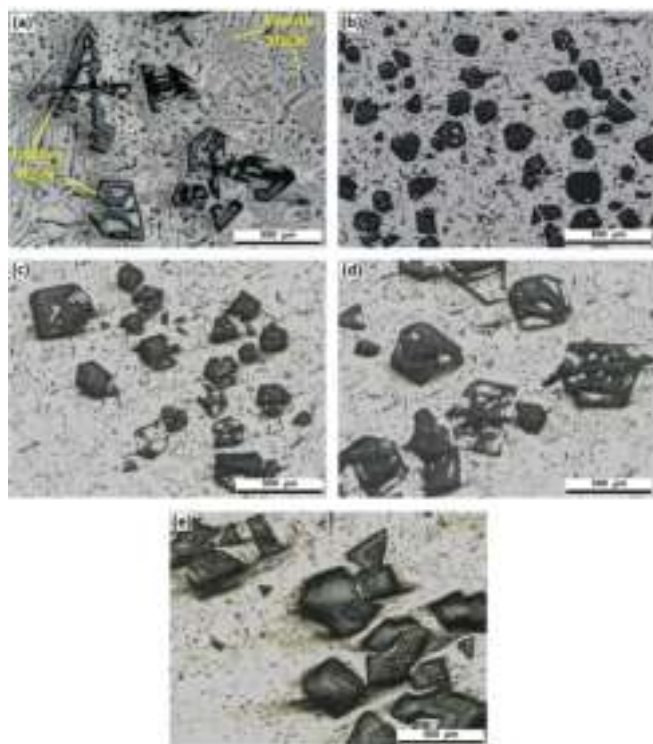
Table 1
Chemical composition of Al–Mg_2Si–2Cu composite used in the present study (wt. %).

Mg	Si	Cu	Fe	Zn	Mn	Pb	Al
12.50	6.82	2.01	0.86	0.59	0.27	0.002	Balance

Fig. 1. Optical microstructures of Al–20Mg$_2$Si–2Cu composites contain different with different Sr content: (a) 0, (b) 0.01, (c) 0.04, (d) 0.08 and (e) 0.1 wt%.

irregular coarse primary structure (Fig. 1a) transformed to semi-tetrakaidecahedron fine shape (Fig. 1b) after addition of 0.01 wt% Sr. It has been reported that {1 1 1} planes grow more rapidly and thus leave {1 0 0} planes resulting in the formation of tetrakaidecahedron [2]. With addition of Sr the size of primary Mg$_2$Si particles decreased and their morphology exhibited a finer structure typical of modification. Similar observations have been reported by Zhao et al. [1] and Qin et al. [2] with addition of 0.05 wt% Sr. However, when the Sr addition increased to 0.1 wt% the structure of primary particles reverted to their coarse morphology indicating a loss of the effect of modification (Fig. 1e).

The details of the microstructural parameters of primary Mg$_2$Si, including the average size, average density, average aspect ratio and average area fraction were determined by examining the corresponding metallography of samples using an image analyser are shown in Table 2. The aspect ratio represents the ratio of the maximum length to the minimum length of the primary Mg$_2$Si particle. It is evident that the average size decreased from $179.40 \pm 14.02 \, \mu m$ to $125.60 \pm 12.34 \, \mu m$ with addition of 0.01 wt% Sr. However, when the amount of Sr addition exceeded 0.01 wt%, the average size increased again and reached a value of $146.60 \pm 16.33 \, \mu m$ with addition of up to 0.1 wt%. The highest

Table 2
Quantitative metallography results for primary Mg$_2$Si particles of the as cast Al–Mg$_2$Si–2Cu in-situ composite with different contents of Sr.

Sr content (wt.%)	Average size of Mg$_2$Si (μm)	Average density of Mg$_2$Si (Particle/mm^2)	Average of aspect ratio	Average of area fraction (%)
0	179.40 ± 14.02	12.54 ± 2.10	1.20 ± 0.04	27.24 ± 3.57
0.01	125.60 ± 12.34	35.50 ± 1.15	1.13 ± 0.04	28.97 ± 2.44
0.04	133.20 ± 14.50	9.51 ± 3.82	1.17 ± 0.03	26.33 ± 2.20
0.08	146.22 ± 14.10	7.61 ± 2.65	1.21 ± 0.04	30.23 ± 3.80
0.1	146.60 ± 16.33	5.38 ± 2.40	1.21 ± 0.06	33.20 ± 4.05

average density (35.50 ± 1.15 particle/mm^2) was obtained for the composite treated with 0.01 wt% Sr, while the lowest value measured was for the composite treated with 0.1 wt% at 5.38 ± 2.40 particle/mm^2.

The area fraction of the primary Mg$_2$Si phase in Al–20Mg$_2$Si–2Cu composite was measured at 27.24 ± 3.57%. It is observed that the area fraction increased slightly to 28.97 ± 2.44% and then decreased to 26.33 ± 2.20% with addition of 0.01 and 0.04 wt% Sr respectively. With further increase to 0.08 and 0.1 wt% Sr, the area fraction increased to 30.23 ± 3.80 and 33.20 ± 4.05 respectively. From Table 2, it can be seen that the density of particles changed significantly compared to the area fraction changes. In fact the effect of Sr addition on the density of primary Mg$_2$Si particles is more discernible than that of area fraction.

The aspect ratio of the untreated composite was measured at 1.20 ± 0.04 and this value decreased to 1.13 ± 0.04 after addition of 0.01 wt% Sr, with the highest value of 1.21 was recorded for the composite treated with 0.08 wt% Sr and 0.1 wt% Sr.

Fig. 2 illustrates the deep etched microstructures of eutectic Mg$_2$Si phase in as-cast Al–20Mg$_2$Si–2Cu composites with different amounts of Sr. Removing aluminium phase by deep-etching helps to better understand the 3-dimensional morphologies of eutectic phase. For the Mg$_2$Si eutectic structure, plate-like structure was observed in the untreated composite (Fig. 2a). With addition of 0.01 wt% Sr, the eutectic morphology exhibited a fine flake structure as shown in Fig. 2b, with further refinement of this flake structure with increased Sr content up to 0.1 wt% (Fig. 2c). The inset image of Fig. 2c shows the new morphology of eutectic Mg$_2$Si having a cubic structure. This type of structure has not been reported in previous research papers which focused on the modification of primary phase with modifier elements.

As seen in Fig. 1, modification of the primary Mg$_2$Si and refinement of eutectic Mg$_2$Si occurred after addition of Sr. However, the mechanism responsible for the modification and de-modification of the primary Mg$_2$Si as well as refinement of eutectic Mg$_2$Si addition of Sr is not clear. According to research findings on the modification of silicon in Al–Si alloys, it has been suggested that the anisotropic growth of the primary Mg$_2$Si particle is impeded by the adsorption of Sr atoms on the forehead growth interface of Mg$_2$Si phase [1]. However, most studies carried out on the modification mechanism of primary Mg$_2$Si particles suggested to the nucleation stage. Indeed, EPMA results showed that AlP particles act as nuclei for the primary Mg$_2$Si [8]. The formation of Bi–Mg and Sb–Mg compounds before the precipitation of primary Mg$_2$Si particles is likely to provides sites for heterogeneous nucleation of the Mg$_2$Si and as a result may induce its modification [9,10]. The absorption of Sr has been reported to be the main reason for the refinement and morphology change of Mg$_2$Si phase [4]. Yang Ming-Bo [3] mentioned that the disregistry at (100)Al$_4$Sr//(100)Mg$_2$Si is low enough for modification to occur. In order to monitor phase evolutions during solidification of MMCs, the recorded cooling curves were analysed. Fig. 3a shows an assembly of cooling curves obtained for an Al–20Mg$_2$Si–2Cu composite treated with various contents of Sr. During solidification of Al–20Mg$_2$Si–2Cu composite five different reactions occur: formation of the primary Mg$_2$Si, eutectic Al–Mg$_2$Si, followed by Al$_5$FeSi and simultaneous precipitation of Al$_5$Cu$_2$Mg$_8$Si$_6$ and Al$_2$Cu intermetallic phases [11]. The magnified area for the formation of primary Mg$_2$Si is illustrated in Fig. 3b. It is clear that the nucleation temperature for the formation of primary Mg$_2$Si increased with addition of 0.01 wt%, and then decreased continuously with increasing Sr content up to 0.1 wt% Sr. In other words, nucleation of primary Mg$_2$Si occurs sooner and easier with addition of 0.01 wt% Sr, which means there are more nuclei during nucleation of the primary Mg$_2$Si phase.

The decrease in the nucleation temperature can be related to the decrease of nucleation probability and therefore in this condition system needs more undercooling to stabilize the nuclei of primary Mg$_2$Si particle. So, it seems that there is direct relationship between nucleation temperature and nucleation sites or density of Mg$_2$Si particles.

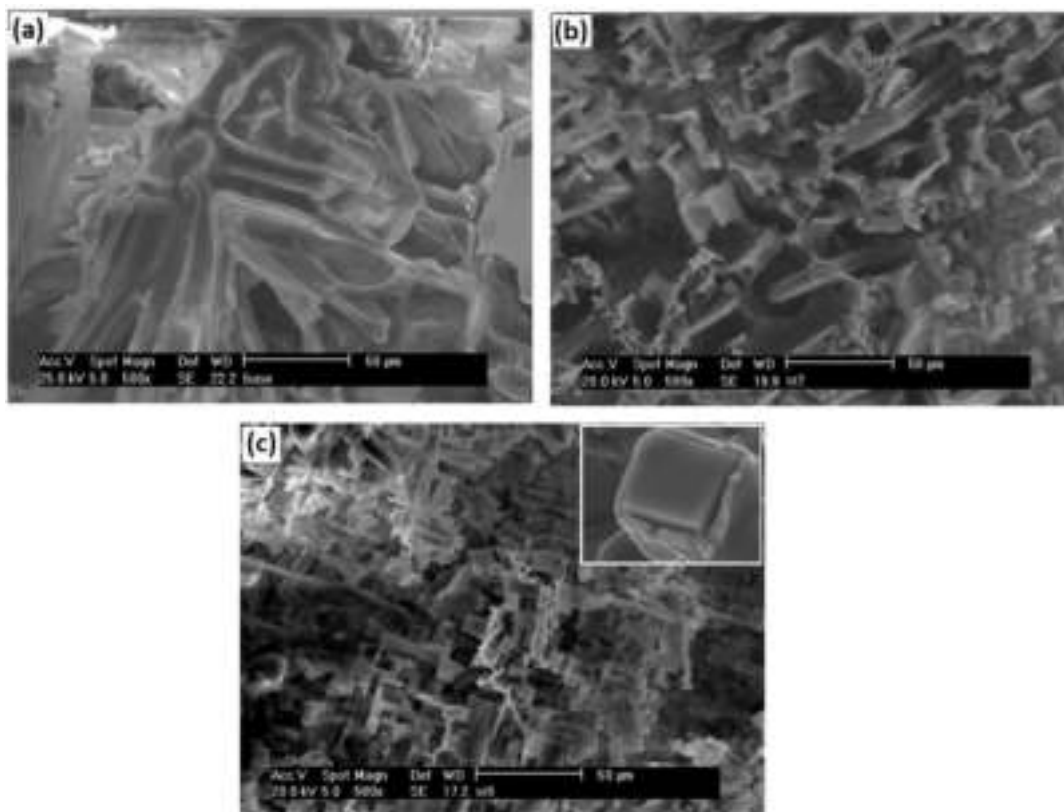Based on thermal analysis results a new peak was detected after the

Fig. 2. Deep-etched microstructures of eutectic Mg_2Si phase with different Sr content: (a) 0, (b) 0.01 and (c) 0.1 wt %.

formation of primary Mg_2Si as indicated by #1 in Fig. 3b for 0.04 wt% treated composite. Fig. 3c is the magnified area of the Al–$20Mg_2Si$–2Cu eutectic reaction showing a depression in the growth temperature of eutectic phase and as a result refinement of eutectic Mg_2Si is obtained. The variations of the nucleation temperature of primary Mg_2Si and the growth temperature of eutectic Mg_2Si in the composites contain various contents of Sr are shown in Table 3. The biggest reduction in the growth temperature of eutectic phase was found in the 0.1 wt% Sr treated composite, which is consistent with the finest eutectic structure as shown in Fig. 2c. Furthermore, the recalescence, that is difference between minimum temperature and growth temperature, increased with increased Sr content. This is indication that the refinement of the eutectic Mg_2Si is most likely associated with the growth rather than the nucleation stage. In addition, another phase was detected (labelled #2) after the formation of phase labelled #1 and prior to the precipitation of the eutectic Mg_2Si phase. Indeed, two different Sr-compound phases were detected based on the obtained cooling curves. It has been reported that addition of Sr more than a certain amount in Al–Si–Mg system causes the formation of Al_2Si_2Sr [12,13].

These Al_2Si_2Sr particles are shown as white particles under backscattered electron microscopy distributed in the microstructure as shown in Fig. 4. Oxide bifilm theory proposed by Campbell [14] can be considered in order to explain the mechanism responsible for the current modification of primary Mg_2Si particles. The oxide biofilm theory states that intermetallic compounds or second phases may nucleate and grow on oxide bifilms suspended in the melt. Thus, it can be suggested that addition of Sr in an amount exceeding 0.01 wt% to Al–Mg_2Si in-situ composite prevents easy nucleation by preventing the oxide film acting as a substrate for nucleation. However, this theory is not reconciled well with increase of nucleation temperature and density of primary Mg_2Si particles.

Xia and Li [15] found that the Al_4Sr particle can be an effective heterogeneous nucleation substrate for Mg_2Si using thermodynamic

analysis and confirmed by EDS and XRD analyses. If this approach is followed carefully, it seems that the increase of nucleation temperature and density of primary Mg_2Si particle show the modification of the primary Mg_2Si is related to the nucleation rather than the growth stage. However, in the present work, no reaction was detected prior to the precipitation of primary Mg_2Si, maybe due to minor amount of Al_4Sr which cannot be distinguishable on derivative cooling curve. Since the formation of these two Sr-compounds (#1 and #2) occurs after the nucleation of primary Mg_2Si but before formation of the eutectic Mg_2Si, it can be the reason for the loss of modification effect of the primary Mg_2Si observed in Fig. 1. They shorten the time and temperature interval for formation of primary Mg_2Si. On the other hand, the eutectic Mg_2Si structure was modified with Sr amount more than 0.01 wt% Sr in the current study. This observation appears to suggest that with Sr additions exceeding more than the best value in this study (0.01 wt%) a certain amount of Sr is used for the modification of the eutectic Mg_2Si and the remainder would likely participate in the formation of Al_2Si_2Sr rather than all the Sr added being used to refine the eutectic Al–Mg_2Si structure.

3.2. Mechanical properties

Fig. 5a shows the engineering stress-elongation curves for the untreated and Sr-treated composites. The details of stress-strain curves including the ultimate tensile strength (UTS) and elongation percentage to failure (El %) are shown in Fig. 5b. The results show that the UTS of untreated composite was 83.2 ± 1.8 MPa which significantly increased to 101.5 ± 1.7 MPa with addition of 0.01 wt% Sr. However, there was a reduction in UTS with increased Sr addition. With 0.04 wt % Sr, the UTS was 86.9 ± 1.9 MPa, which decreased to 76.5 ± 1.7 MPa for 0.08 wt% Sr, and then to 75.7 ± 1.3 MPa with the addition of 0.1 wt% Sr. The results in Fig.5b also show that when the composite was treated with 0.01 wt% Sr, El% increased from $0.78 \pm 0.08\%$ to $1.1 \pm 0.04\%$. With
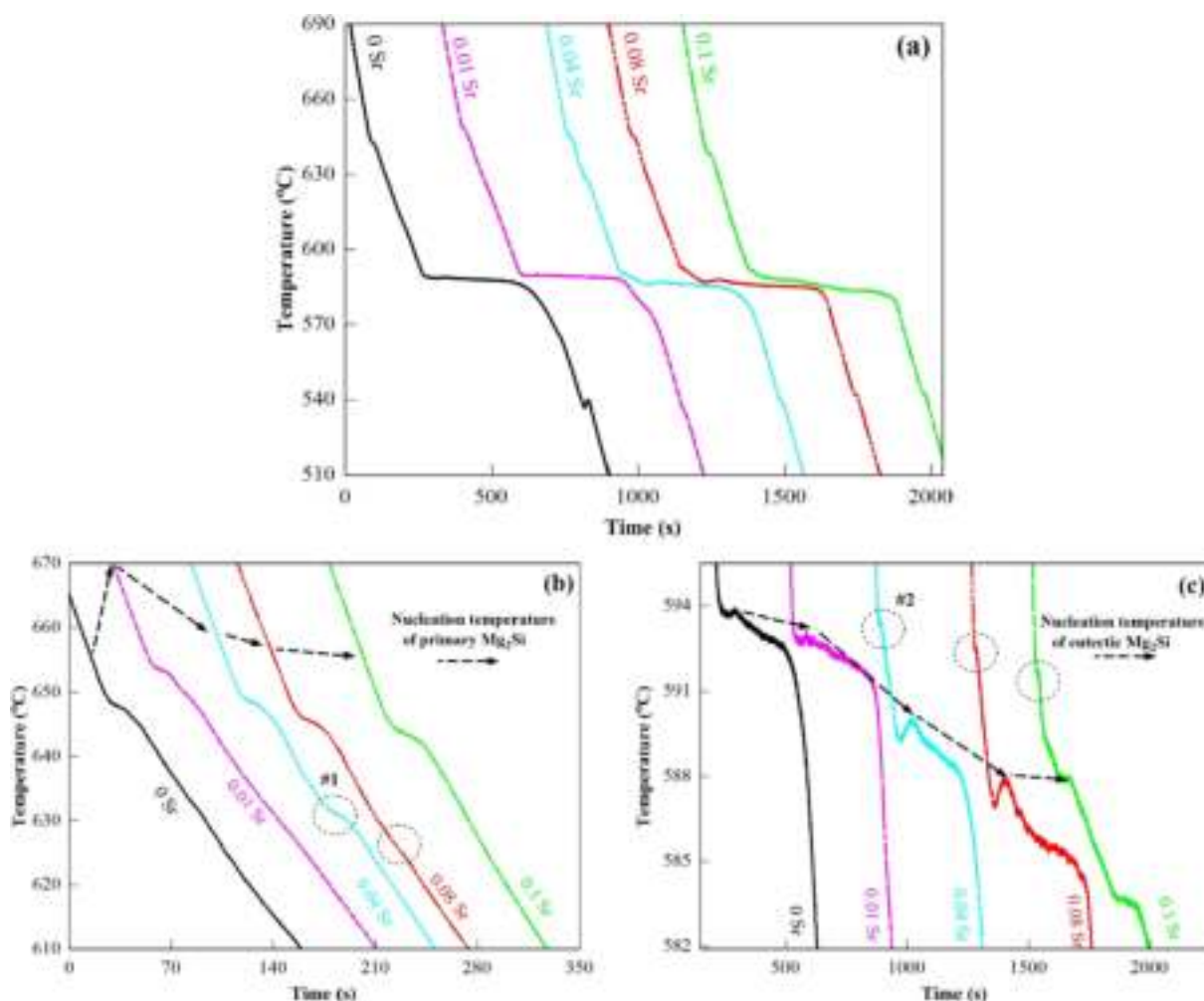
Fig. 3. (a) assembly of cooling curves for different Sr addition levels to the Al–20Mg$_2$Si–2Cu in-situ composite. The magnification of area related to the onset of (b) primary and (c) eutectic Mg$_2$Si.

Table 3
Nucleation temperature of primary Mg$_2$Si and growth temperature of eutectic Mg$_2$Si as a function of Sr content.

Temperature (°C)	Sr content (wt.%)				
	0	0.01	0.04	0.08	0.1
Nucleation temperature of primary Mg$_2$Si	657.3	670.3	658.9	657.8	657
Growth temperature of eutectic Mg$_2$Si	593.8	592.9	589.9	587.9	588

increasing Sr content in the composite, however, El% decreased to 0.96 ± 0.06%, 0.74 ± 0.06% and 0.6 ± 0.06% % after addition of 0.04, 0.08 and 0.1 wt % Sr respectively. The lower UTS and El% values of the Al–20Mg$_2$Si–2Cu composite for higher Sr addition can be ascribed to the presence of brittle Al$_2$Si$_2$Sr compound in the microstructure of composite with 0.08 and 0.1 wt% Sr (Fig. 4). Al$_2$Si$_2$Sr compound tends to crack early during plastic deformation, lowering the strength and ductility of the composite.

Fig. 5c shows the results of impact toughness values of the composites without and with addition of Sr. The toughness of composite without Sr was measured at 0.82 ± 0.16 J which increased to 1.31 ± 0.12 J after addition of 0.01 wt% Sr. The impact toughness decreased to 1.14 ± 0.12 J, 0.8 ± 0.16 J and 0.76 ± 0.10 J with additions of Sr to 0.04, 0.08 and 0.1 wt % Sr respectively. The effect of Sr addition on the hardness is illustrated in Fig. 5c. The highest hardness was observed in the composite treated with 0.01 wt% Sr at 81 ± 3 HVN

Fig. 4. EDS analysis results for white particle.

compared with the treated composite (66.5 ± 2 HVN). The hardness was then decreased with increasing the Sr content but was always higher than the hardness of the untreated composite. The changes in the hardness values with addition of Sr are attributed to the change in average size and density (Table 2) and morphology of primary and

Fig. 5. (a) Engineering stress versus strain curve, (b) extracted UTS and El% and (c) impact toughness and hardness of the Al–20Mg$_2$Si–2Cu composites containing different Sr contents.

eutectic Mg$_2$Si phases (Fig. 1). Change in the morphology of Mg$_2$Si reduces stress concentration resulting in an improvement in the bonding between reinforcement and matrix. Moreover, improvement in hardness with Sr additions can be associated with the finer and hard primary phases floating in the matrix.

3.2.1. Fractography of tensile samples

The mechanical behaviour and fracture surfaces of the composite were examined with the SEM. Fig. 6 illustrates SEM micrographs of fractured Al–20Mg$_2$Si–2Cu tensile samples treated with different amounts of Sr at low (a, c, e and g) and high (b, d, f and h) magnifications. Okabayashi et al. [16] stated that the crack propagation behaviour is governed by the primary Si particles in Al–Si hyper-eutectic alloy, which is similar to the primary Mg$_2$Si particles Al–20Mg$_2$Si composite, where the cracks propagate by the successive cleavage of these particles.

Fig. 6a shows the fracture surface of the composite without Sr addition where it is seen that the primary Mg$_2$Si exhibits a coarse morphology with sharp edges, which may trigger cracks to initiate in the Mg$_2$Si particles. Once a crack is initiated, it will propagate to the eutectic Al–Mg$_2$Si matrix leading to failure. The sharp edges and inherent brittleness of Mg$_2$Si caused local stress concentrations, resulting in cracking

of the Mg$_2$Si particles. Fig. 6b clearly shows decohesion of particles as well as debonding at the interface between Mg$_2$Si particles and matrix, which indicates weak bonding strength at the matrix/reinforcement interface. Such an observation on may be reconciled with the lower UTS and El% values obtained (Fig. 5b). When the composite was treated with 0.01 wt% Sr (Fig. 6c and d) the Mg$_2$Si particles exhibit fine morphology on the fracture surface with less decohesion but more cracking of particles. Indeed, the composite that was treated with 0.01 wt % Sr showed the highest UTS and El% values. This is probably attributed to the decrease in aspect ratio of the Mg$_2$Si as shown in Table 2 or in other words to the increase in sphericity of the Mg$_2$Si. In this case, the number of sites where stress may concentrate are reduced and crack propagation is slowed down. Additionally, a low aspect ratio and better sphericity of Mg$_2$Si particles increases composite resistance to fracture due to the effect of Mg$_2$Si particles on the first stage of the crack, i.e., void nucleation, resulting in increase of El% and impact toughness of the composite containing 0.01 wt % Sr.

As the amount of Sr added is increased more decohesion and cracking of particles can be seen on the fracture surfaces as shown in Fig. 6c and d for 0.04 wt % Sr and 0.08 wt% Sr respectively. As discussed above, increasing the amount of Sr addition causes de-modification and

Fig. 6. SEM fractographs of Al–20Mg$_2$Si–2Cu tensile samples with different contents of Sr at low (left) and high (right) magnifications: (a, b) 0, (c,d) 0.01, (e, f) 0.04 and (g, h)0.1 wt% Sr.

coarsening of the primary Mg$_2$Si particles, whose presence act as stress concentration sites leading to initiation of cracks. The composite treated with the highest amount of Sr (0.1 wt%) exhibited brittle fracture as shown in Fig. 6e resulting in the lowest impact energy. It is evident from the observed fracture surfaces that the presence of coarse primary Mg$_2$Si particles provides potential sites for crack initiation and decrease the impact energy. These results are consistent with the quantitative analysis results of the primary Mg$_2$Si particles given in Table 2.

Using numerical analysis and the finite element method, Saigal and coworkers [17] found that the inhomogeneity in stress and strain in two-phase Al–Si alloys increases as the microstructure becomes coarser and the particle size increases. The flow stress of a coarse dispersion of Si

particles in an Al matrix will be lower than a fine dispersion. On the other hand, As the volume fraction of particles increases, the stress concentrations produced in the particles decrease. So, the large particles are more susceptible to cracking [18] and the stress required to break a particle is inversely dependent on the particle size [17]. Decreasing the aspect ratio or the particle size and increase of particle density and volume fraction for 0.01 wt% Sr increases the crack initiation stress and has a beneficial effect on elongation and impact toughness and increased them by about 41% and 31% respectively.

On the other hand, the low ductility and UTS of the Al–20Mg$_2$Si–2Cu composite for higher Sr addition can be attributed to the presence of brittle Al$_2$Si$_2$Sr (Fig. 4) in the composite containing 0.04, 0.08 and 0.1 wt

% Sr. It is worth noting that the volume fraction of Al_2Si_2Sr increased with increase of Sr addition. These compounds tend to crack early during plastic deformation, lowering the strength and ductility of the composite.

3.3. Wear properties

In order to evaluate the sliding wear behaviour of the composites under dry conditions, a comparison was made between the different Sr additions. The changes in weight loss of fabricated composites based on sliding distance under loads of 5 N and 20 N are plotted in Fig. 7a and b respectively. As can be seen, the weight loss increased linearly with increasing sliding distance for all composites investigated. In addition, the weight loss of Sr treated composites was found to be smaller than that of the composite without Sr. Similarly, Fig. 7c shows the corresponding wear rates of composites for different Sr additions under loads of 5 N and 20 N. It is evident that there is a single relationship of wear rate for all composites and for both applied loads. Furthermore, the wear rate was observed to decrease significantly with the addition 0.01 wt% Sr, but then slightly increased with further additions of Sr. These results are consistent with the measured hardness (Fig. 5c) and archard equation (Eq. (2)).

$$Q = \frac{KW}{H} \tag{2}$$

Where Q is wear rate (mm^3/km), W is the volume of worn material per distance, K is a constant called wear coefficient and H is the hardness of the specimen in Vickers scale (kgf/mm^2) [19]. Hardness of the composite increased with increasing the density of Mg_2Si reinforcement particles and as a result, the depth of penetration by the harder asperities

of hardened steel disk is primarily governed by the protruded hard Mg_2Si particles. Thus, the 0.01 wt % Sr treated composite with a higher density of finely dispersed Mg_2Si particles exhibits the highest wear resistance. The role of reinforcement particles is to support the contact stresses preventing high plastic deformation and abrasion between the contact surfaces and hence reducing the amount of worn material [20]. As reported by Sun [21] factors such as type, size and volume fraction of reinforcement particles may influence wear of the composites. The wear resistance is generally improved by increasing the particles size [22–25]; however, in the present work results showed that it has not been improved and even decreased if delamination and/or particle fracture occurs. The interface of Mg_2Si and Al matrix is prone to cracking especially when the particle size is increased [26]. The small size of Mg_2Si particles in the 0.01 wt % Sr treated composite reduces the stress concentration at the matrix/particles interface. Indeed, the present results clearly show that the change in particles size of Mg_2Si (Table 2) is as a key parameter influencing the wear resistance rather than the hardness and reconcile well with previous studies [27]. As a result, the composite treated with 0.01 wt% Sr has the highest wear resistance. When Sr additions are increased up to 0.1 wt % led to a decrease in wear resistance. Fig. 7 also shows that both weight loss and wear rate increase when the load applied increases from 5 N to 20 N for all composites. The higher wear rates observed at 20 N are attributed to the fact that at higher loads the stress induced on the wear surface is higher, meaning the number of contact asperities increases and as a result the material surface wears faster [27].

Fig. 8(a–f) depict the variation of friction coefficient (μ) values of composites without and with 0.01 wt % and 0.1 wt % Sr under applied loads of 5 N and 20 N. Results show that the average friction coefficient

Fig. 7. Wear weight loss versus sliding distance for Al–20Mg2Si–2Cu MMCs with varying contents of Sr under (a) 5 N and (b) 20 N and (c) corresponding wear rates of MMCs versus different contents of Sr under different loads.

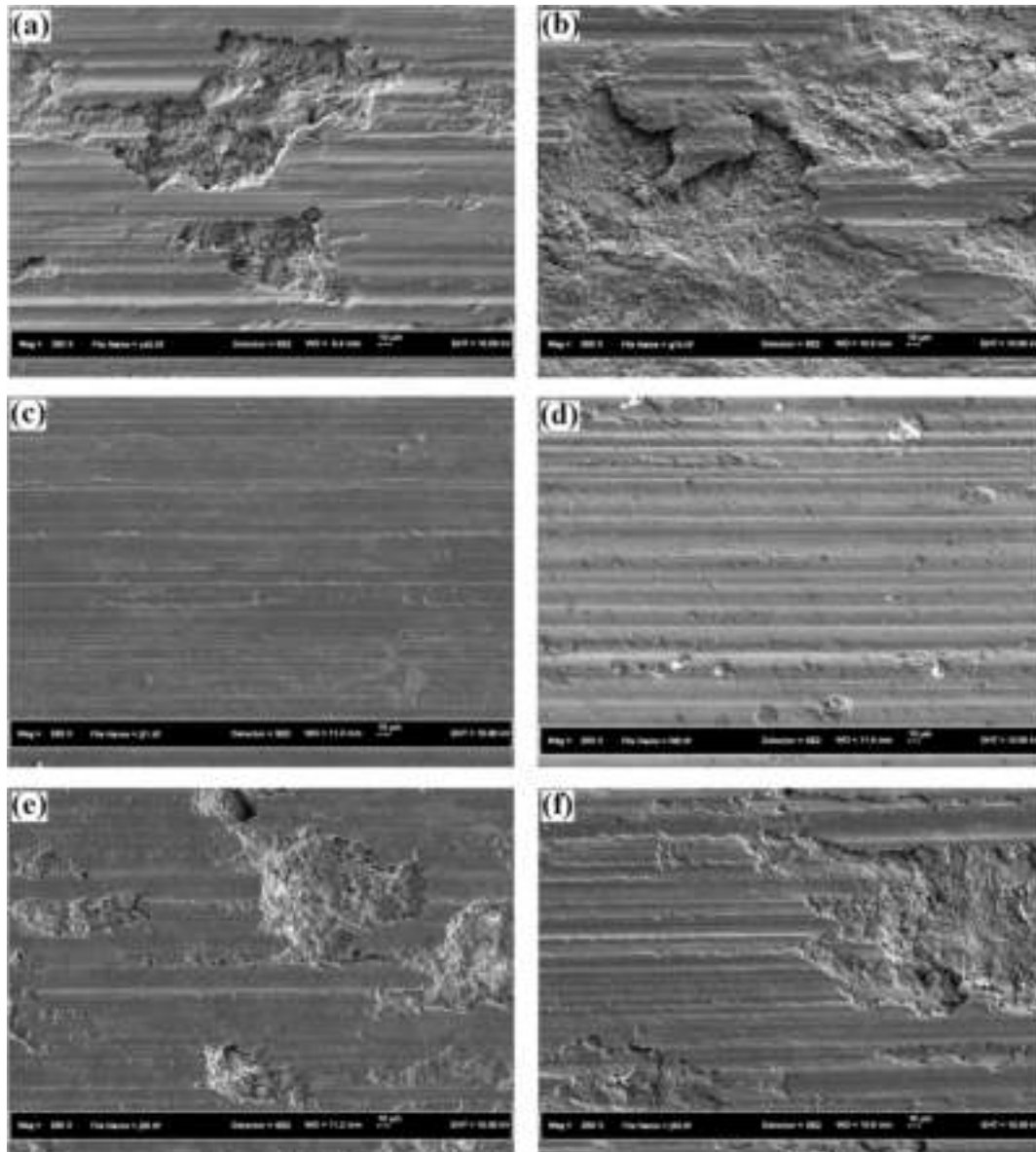**Fig. 8.** Change in the coefficient of friction versus sliding distance for MMCs with (a, b) 0 wt% Sr, (c, d) 0.01 wt % Sr, and (e, f) 0.1 wt % Sr under 5 N (left) and 20 N (right).
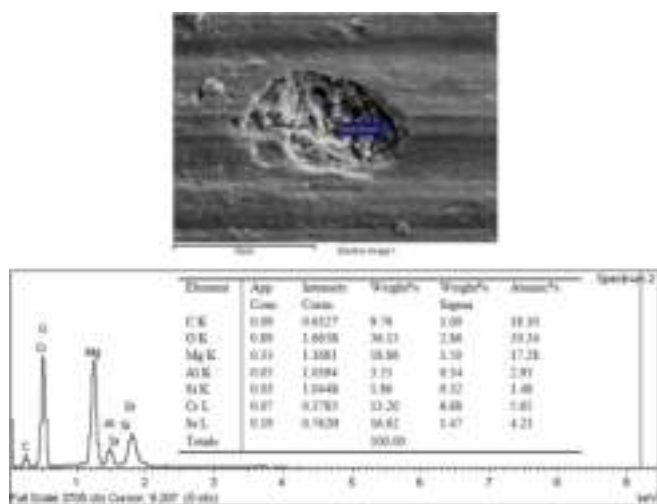
of untreated composite under 5 N load was found to be 0.55 which is greater than that of the 0.01 wt % Sr treated composite (0.52). The higher value of the untreated composite is probably due to fracture of the coarse dendritic Mg₂Si primary phase and plate-like eutectic Mg₂Si into small particles during sliding. These particles may not be able to support the applied load in order to reduce the touching area between the pin and disk. Moreover, Mg₂Si particles lose their effectiveness to resist deformation developed on the worn surface, and as a result cracks can propagate through the matrix leading to pull-out of the Mg₂Si from the matrix. When this pull-out occurs, the Mg₂Si may act as hard abrasive particles against the composite. As illustrated in Fig. 8, the composite treated with 0.01 wt % Sr has the lowest friction coefficient and that wear appears to be predominately abrasive and adhesive which is

consistent to its corresponding lower mass loss (Fig. 7). This is due to the high value of hardness of the material since the protruded Mg₂Si particles can withstand the applied load, with a decrease in the touching area between the pin and counterpart, which results in a decrease in friction coefficient [28–30]. However, when the Sr content is at a higher value of 0.1 wt %, the Mg₂Si particles become larger and the friction coefficient increased (0.54). Another feature of Fig. 8 is the fact that when the applied load increases from 5 N to 20 N the friction coefficient values showed no significant change. Nevertheless, the friction coefficient under an applied load of 20 N is a bit higher as shown in Fig. 8.

The FESEM images of the worn surfaces of untreated and Sr treated composites under 5 N and 20 N applied loads at a sliding distance of 2000 m are shown in Fig. 9(a–f) which illustrate the contributed wear

mechanisms. The worn surface of composite without Sr shows deep and wide ploughing grooves parallel to the sliding direction indicating that abrasion accompanied with delamination is the main wear mechanism (Fig. 9a). The ploughing grooves are caused by fracture of the coarse dendritic primary Mg_2Si which were pulled out from the matrix would increase the depth of wear grooves with a non-uniform distribution. In addition, delamination is caused by the fracture of coarse plate-like eutectic Mg_2Si because of the imposed stress on the worn surface during the wear test. With an increase in load, the composite with no Sr exhibited mainly adhesion wear with delamination of material pickup on the worn surfaces being observed. Higher amount of material removal, which is consistent with the higher value of coefficient of friction and extensive pits indicating severe wear mechanism when the load was, increased (Fig. 9b).

With the addition of 0.01 wt % Sr, the worn surface of the composite has a rather smooth appearance with narrow grooves and shallow pits, which is most likely due to the presence of the fine and uniformly distributed hard Mg_2Si particles in the matrix. In addition, the tendency of primary Mg_2Si to fracture decreased leading to more effective wear load distribution [31]. It is clear from the observations that the

composite treated with 0.01 wt % Sr exhibits higher wear resistance compared to that of the composite without Sr. Refinement of the eutectic Mg_2Si phase may also have played an important role in decreasing the wear rate as it forms a rough interface with the matrix which may suppress initiation and propagation of cracks, and as a result enhancing the wear resistance of Sr treated Al–20Mg_2Si–2Cu composite [32].

Based on the results of coefficient of friction and worn surface of 0.01 wt% Sr treated composite, the dominant wear mechanism appears to be that of mild and sever abrasion as illustrated in Fig. 9c and d respectively. However, with increasing Sr addition up to 0.1 wt %, delaminated areas and wide ploughing grooves appear again (Fig. 9 e), but are smaller than those observed in the composite without Sr. It is possible that the presence of hard Al_2Si_2Sr intermetallic compound in the composite containing higher level of Sr (0.1 wt % Sr) may also contribute to wear resistance compared to the composite without Sr. Indeed, Fig. 10 shows the presence of such Sr compound on the worn surface of 0.1 wt% modified composite under 5 N applied load. Similar findings have been reported by Wu et al. [5] for Nd-modified Al–18% Mg_2Si in situ composite. As shown in Fig. 9f, by increasing the load to 20 N, the wear mechanism of 0.1 wt % Sr changed to sever abrasion and

Fig. 9. Comparison of FESEM images for MMCs with (a, b) 0 wt % Sr, (c, d) 0.01 wt % Sr, and (e, f) 0.1 wt % Sr under 5 N (left) and 20 N (right).

Table 4
Polarisation data of Al–Mg$_2$Si–2Cu-xSr in 3.5% NaCl solution.

Sr content (wt.%)	E$_{corr}$ vs. SCE (V)	I$_{corr}$ (µAcm^{-2})
0	−1090.3	0.732
0.01	−1040.8	0.495
0.04	−1107.8	0.583
0.08	−1091.7	1.280
0.1	−1164.7	1.881

Fig. 10. The presence of (a) Sr compound on the surface of composite treated with 0.1 wt % under applied load of 5 N and (b) corresponding EDS analysis of Sr compound.

delamination wear. This can be explained by the fact that when the load is higher, the soft Al matrix smears off resulting in higher wear even with the presence of Mg$_2$Si particles and Al$_2$Si$_2$Sr compound. Moreover, a large amount of abrasive particles were observed to have embedded in the cavities, which provided scratching action compared to the samples tested under a lower load of 5 N.

3.4. Corrosion behaviour

The results of polarisation test for Al–20Mg2Si–2Cu in-situ composite with different amounts of Sr are presented in Fig. 11, which clearly shows that addition of Sr can change the corrosion resistance of the composite. It can be seen that no passivation or pseudo passivation phenomena were observed indicating an active mechanism of Al–20Mg2Si–2Cu dissolution. According to Fig. 11, no definite trend was observed in the shift of polarisation curves in the presence of different amounts of Sr. The electrochemical kinetic parameters such as corrosion potential (E$_{corr}$) and corrosion current density (i$_{corr}$) are given in Table 4. Corrosion current density of Al–20Mg2Si–2Cu was found to be 0.73 µA/cm^2, meanwhile with the addition of as much as 0.01% Sr this value decreased to 0.49 µA/cm^2. It has been reported that corrosion properties of Al alloys are principally dependent upon the chemical

composition, size, and number of the precipitates [33,34]. The decrease in corrosion current density could be attributed to the presence of fine and uniformly distributed Mg$_2$Si particles which restrict the propagation of corrosion pits [6,35]. From Table 4, the corrosion current density increased to 1.28A/cm^2 when the composite was treated with 0.1 wt% Sr due to coarsening of the Mg$_2$Si particles. The present results suggest that the best value of Sr in this study required to refine the Mg$_2$Si particles and enhance the corrosion resistance based on Stern-Geary equation [36] is 0.01 wt % of Sr.

An immersion test has also been conducted to determine the corrosion rate of Al–20Mg2Si–2Cu in-situ composites for a duration of 25 days. The weight loss data was collected from the immersion test and is as shown in Fig. 12. It can be seen from Fig. 12 that additions of Sr amounts exceeding 0.01 wt% produce higher weight loss. However, it is evident that a smaller amount of 0.01% wt. Sr results in minimal weight loss compared to all composites with and without Sr. The weight loss results can be correlated with the microstructures observed and the fact that the composite treated with 0.01 wt% Sr was shown to refine the Mg$_2$Si particles, it resulted in the lowest weight loss and corrosion rate and hence a better corrosion resistance.

To better understand the corrosion behaviour of Al–20Mg2Si–2Cu composite, the corroded surfaces of samples with 0.01 wt% (the best value in this study) and higher level of Sr (0.08 wt%) immersed in 3.5% NaCl for 5 days were examined under SEM (Fig. 13). It can be seen that the composite with 0.01 wt% (containing finer Mg$_2$Si particle) is subjected to less corrosion attack in comparison to the composite with 0.08 wt % Sr. In fact, Mg$_2$Si particles play the role of cathode during galvanic corrosion with the extended time. Based on their size and distribution, the pitting corrosion decreased and the rate of corrosion diminished. Similar findings have been reported by Zedi Li et al. [6].

Two different parameters affect the corrosion behaviour of Al–20Mg2Si–2Cu composite. First, the size and density of Mg$_2$Si particles and second is the formation of second phases. Many researchers have reported that by transforming Mg$_2$Si from enormous dendrites to fine and uniformly distributed polyhedron, the corrosion pits propagating

Fig. 11. Polarisation curve of Al–Mg$_2$Si–2Cu-xSr in 3.5% NaCl solution.

Fig. 12. wt loss and corrosion rate of Al–20%Mg$_2$Si–2Cu composites containing different Sr contents in 0.5 M H$_2$SO$_4$ solution.